Time Entanglement between a Photon and a Spin Wave in a Multimode Solid-State Quantum Memory

Kutlu Kutluer,[1] Emanuele Distante,[1] Bernardo Casabone,[1] Stefano Duranti,[1] Margherita Mazzera,[1] and Hugues de Riedmatten[1,2]

[1]*ICFO-Institut de Ciencies Fotoniques, The Barcelona Institute of Science and Technology, Mediterranean Technology Park, 08860 Castelldefels (Barcelona), Spain*
[2]*ICREA-Institució Catalana de Recerca i Estudis Avançats, 08015 Barcelona, Spain*

The generation and distribution of entanglement are key resources in quantum repeater schemes. Temporally multiplexed systems offer time-bin encoding of quantum information which provides robustness against decoherence in fibers, crucial in long distance communication. Here, we demonstrate the direct generation of entanglement in time between a photon and a collective spin excitation in a rare earth ion doped ensemble. We analyze the entanglement by mapping the atomic excitation onto a photonic qubit and by using time-bin qubit analyzers implemented with another doped crystal using the atomic frequency comb technique. Our results provide a solid-state source of entangled photons with embedded quantum memory. Moreover, the quality of the entanglement is high enough to enable a violation of a Bell inequality by more than two standard deviations.

Light-matter entanglement is an important resource in quantum information science. It enables complementing the advantages of using photons as flying qubits in quantum communication schemes with those of matter qubits, which are ideal for quantum storage and processing [1,2]. It can be achieved, for example, by interfacing quantum sources of entangled photons with long lived quantum memories [3–5]. But the direct generation of light-matter entanglement, without the use of external photon pair sources, is particularly attractive in view of practical application as it generally features less complexity and can lead to higher efficiency than the so-called read-write memory protocols [6].

A very convenient method to directly generate light-matter entanglement in atomic ensembles is the Duan-Lukin-Cirac-Zoller (DLCZ) protocol [7]. It is based on the off-resonant excitation by means of weak classical write pulses of an atomic ensemble with a lambda system. With a small probability, a Raman scattered write photon creates a collective spin excitation, heralded by the emission of a Stokes photon. The spin wave can be converted into a second photon, the anti-Stokes photon, with the use of a strong on-resonant read pulse. In this way, the light-matter entanglement is mapped into photonic entanglement, which can be analyzed with photonic qubit analyzers. Several types of entanglement have been demonstrated using the DLCZ scheme in atomic gases, such as polarization [8,9], spatial modes [10–12], orbital angular momentum [13], and time bin [14]. The DLCZ scheme has also been demonstrated with nanomechanical resonators [15].

The use of atomic ensembles embedded in solid matrices, such as rare-earth-ion-doped (REID) crystals, offers numerous advantages as the coherence times are comparable to those of cold atomic clouds but the natural trapping greatly simplifies the experimental setups. Moreover, the inhomogeneous broadening of the atomic transitions can be used as a resource for quantum information multiplexing [16,17]. However, the standard off resonant DLCZ scheme is difficult to apply to REID crystals, due to the very weak dipole moments of the optical transition. Alternative schemes have been proposed that use resonant excitation and rephasing techniques to counteract the inhomogeneous dephasing of the atomic dipoles [18,19]. Very few attempts of implementing DLCZ-like schemes in REID crystals have been done, demonstrating continuous variable entanglement [20,21] and quantum correlation between photons and spin waves [22,23]. The latter demonstrations combined the DLCZ protocol and the atomic frequency comb (AFC) storage scheme [16].

In this Letter, we use the AFC-DLCZ protocol to create entanglement in time between a single photon and a single collective spin excitation in a REID memory crystal (MC), in the photon counting regime. The matter state is transferred on demand onto a single photon, and the photonic qubits are analyzed in Franson-like interferometers implemented with another REID crystal. The entanglement is demonstrated by observing high-visibility two-photon interference in different bases and by violating a Bell inequality.

In the AFC-DLCZ protocol, a write pulse resonant with an AFC structure with comb spacing Δ is used. Excited
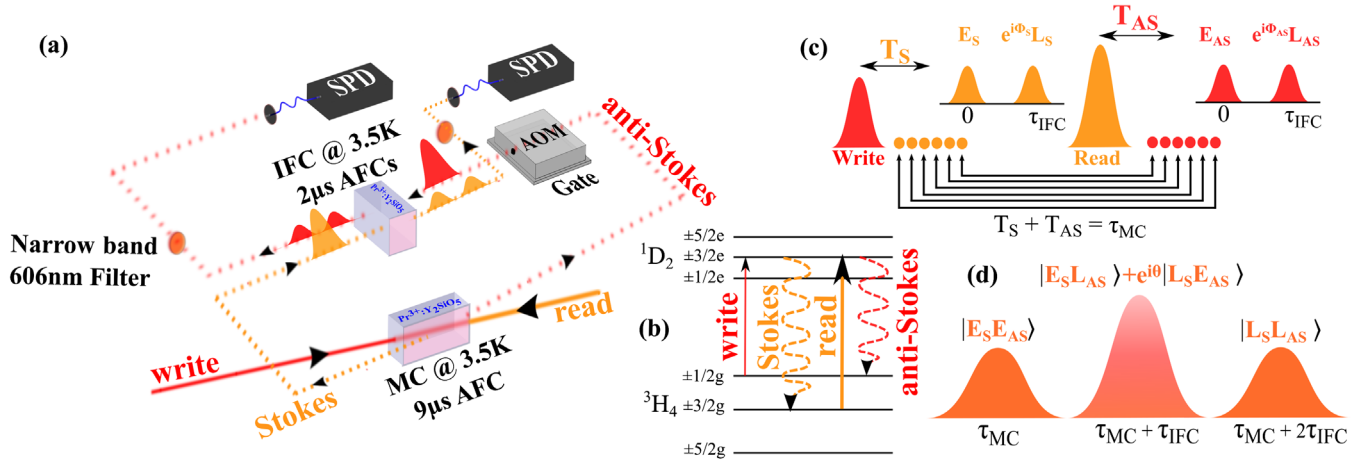
FIG. 1. (a) Experimental setup. The write and read pulses are polarized parallel to the D_2 memory crystal (MC) axis to maximize the interaction. Both Stokes and anti-Stokes photons pass through the interferometric filter crystal (IFC), but in different spatial modes, where dedicated laser beams prepare the required spectral features (transparency window or AFC). Spectral filters at 600 nm (width 20 nm) are placed on both arms before the photons are fiber coupled to the single photon detectors (silicon SPD). (b) Hyperfine splitting of the first sublevels (0) of the ground $^3H_4$ and the excited $^1D_2$ manifolds of Pr^{3+} in Y_2SiO_5. (c) Temporal pulse sequence for the AFC-DLCZ protocol. T_S (T_{AS}) is the time separation between a Stokes (anti-Stokes) photon detection and the write (read) pulse. The insets show the effect of the AFCs in the IFC on the Stokes (orange) and anti-Stokes (red) photons. (d) Sketch of the Stokes–anti-Stokes coincidence histogram vs $T_S + T_{AS}$ when the IFC is prepared with an AFC in each photon arm, with equal transmission and echo probability.

atoms will then start to dephase due to the inhomogeneous broadening. Spontaneously emitted Stokes photons are collected between the write pulse and the corresponding AFC echo, which appears at time $\tau_{MC} = 1/\Delta$. The Stokes photons emitted at different times $T_S < \tau_{MC}$ [where T_S is defined as the time between the write pulse and the Stokes photon emission, see Fig. 1(c)], are correlated to independent spin waves leading to entanglement in time between the Stokes photons and the stored spin waves. The joint light-matter state can be written to first order (not normalized) as

$$|\Psi_{S,SW}\rangle = \int [\mathbb{1} + \rho(T_S) a_S^\dagger(T_S) a_{SW}^\dagger(T_S)]|0_S, 0_{SW}\rangle dT_S, \quad (1)$$

where $a_S^\dagger$ ($a_{SW}^\dagger$) is the creation operator for the Stokes photon (spin wave) and $\rho(T_S)$ the temporal dependency of the wave function [18].

A strong resonant read pulse can be sent at a later time to excite the spin wave back to the excited states, which, after a finite rephasing time given by the AFC, leads to collective emission of an anti-Stokes photon at a time T_{AS} after the read pulse. Because of the fixed rephasing time τ_{MC} of the excited state, the anti-Stokes emission time is correlated with the Stokes emission time following $T_S + T_{AS} = \tau_{MC}$. In the ideal case of unity read-out efficiency, the joint state of the Stokes–anti-Stokes photons $|\Psi_{S,AS}\rangle$ can then be written (not normalized) as

$$\int [\mathbb{1} + \rho(T_S) a_S^\dagger(T_S) a_{AS}^\dagger(\tau_{MC} - T_S)]|0_S, 0_{AS}\rangle dT_S, \quad (2)$$

where $(a_{AS}^\dagger)$ is the creation operator for the anti-Stokes photon. Our device therefore acts as a source of entangled photons with embedded quantum memory.

In this experiment, we use two $Pr^{3+}:Y_2SiO_5$ (Pr:YSO) crystals, a memory crystal (MC), and an interferometric filter crystal (IFC), both cooled down to 3.5 K [22] in a closed loop cryostat. This material offers long coherence times [24], high storage and retrieval efficiencies [25], and prospect for on-chip integration [26,27]. A sketch of the relevant experimental setup and the energy level scheme of Pr^{3+} in YSO are shown in panels (a) and (b) of Fig. 1. We tailor the $1/2_g - 3/2_e$ transition of the MC as an AFC structure with $\tau_{MC} = 9$ μs, while the $3/2_g$ state is emptied to store the single spin excitation (see [28] for more details). We prepare the AFC structures every cryostat cycle (1 Hz rate).

We then start to send Gaussian write pulses resonant to the AFC at a rate of 3.7 kHz (1100 pulses per AFC preparation). We detect the Stokes photons in a 4 μs window starting 1 μs after the write pulse [temporal sequence in Fig. 1(c)]. As discussed in [22], the number of temporal modes stored is given by the ratio between the Stokes photon detection window (limited by τ_{MC}) and the duration of the Stokes photon itself. The latter is set by the duration of the write pulse (700 ns of full width at half-maximum in our case), therefore resulting in five distinguished temporal Stokes modes. The Stokes detection

mode is set to an angle of about 3° in the backward direction with respect to the write mode, to minimize the leakage noise from the write pulse. Conditional on a Stokes photon detection, we send the Gaussian read pulse, counterpropagating to the write mode and delayed by 16 μs. As a consequence of the phase-matching conditions, the Stokes and anti-Stokes photons are emitted in opposite directions. The anti-Stokes detection gate is finally opened for about 10 μs. The average storage time in the spin state is $\bar{\tau}_S = 13$ μs. Directly after the emission, the Stokes photons are steered to the IFC, where a 2 MHz-wide transparency window is prepared, to filter the photons emitted through the decay to hyperfine ground levels other than the $3/2_g$. The anti-Stokes photons are temporally gated with an acousto-optic modulator before traveling through the IFC where another transparency window is created in a different spatial mode to suppress the coherent and incoherent noise deriving from the read pulse [29]. AFCs can also be created in the IFC, which will serve as qubit analyzers for the photons (see below). Both Stokes and anti-Stokes photons are detected with single photon counters (SPD) and their arrival time is saved to reconstruct coincidence histograms.

We first verify that the Stokes and anti-Stokes photons are emitted in pairs, and assess the cross-correlation function $g_{S,AS}^{(2)} = p_{S,AS}/(p_S \cdot p_{AS})$, where $p_{S,AS}$ is the probability to detect a coincidence between a Stokes and an anti-Stokes photon and p_S (p_{AS}) is the probability to detect single Stokes (anti-Stokes) photon. Figure 2 shows the measured $g_{S,AS}^{(2)}$ histogram fixing the coincidence window time-bin size to $\Delta t = 600$ ns. This measurement is taken with a write pulse power of $P_W = 90$ μW, corresponding to a total Stokes creation probability $P_S = 1.6\%$ ($P_S = 0.4\%/\mu$s). We observe a clear peak at $T_S + T_{AS} = 9$ μs, that represents the correlated Stokes–anti-Stokes pairs, featuring a maximum of $g_{S,AS}^{(2)} = 17.3 \pm 3.3$. This is widely above the
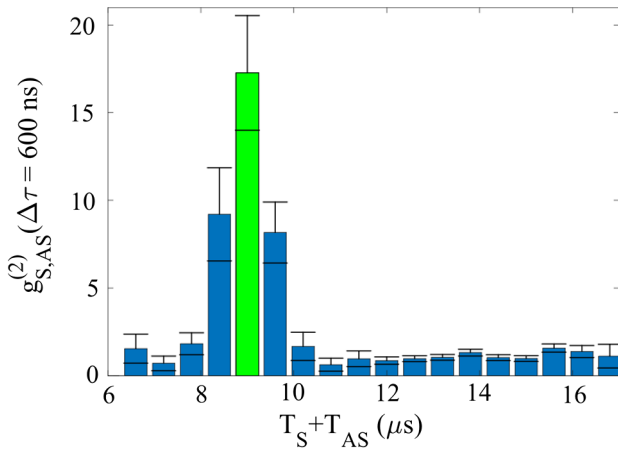
FIG. 2. Typical $g_{S,AS}^{(2)}$ histogram as a function of the $T_S + T_{AS}$ time, with a time-bin size of 600 ns. The write pulse power P_w is 90 μW, corresponding to a Stokes creation probability $P_S = 0.4\%/\mu$s.

classical limit of 2 fixed by the Cauchy-Schwarz inequality, assuming thermal statistics for the Stokes and anti-Stokes fields, as predicted for the DLCZ protocol in the ideal case [30]. The efficiency to retrieve an anti-Stokes photon, conditioned on a Stokes detection, is about 1.6%, mostly limited by the read pulse transfer efficiency, uncorrelated background detection in the Stokes mode, and the rephasing efficiency of the AFC and spin-wave decoherence [22,31]. To further characterize our system, we measured the coincidence count rate and $g_{S,AS}^{(2)}(\Delta t = 600$ ns) as a function of the Stokes probability P_S [31]. For a similar value of $g_{S,AS}^{(2)}$, we achieve a coincidence count rate 8 times higher than in our previous demonstration [22], thanks to a larger number of trials per comb, to an increased optical transmission between the MC and the IFC, and to a larger Stokes detection window [31].

To demonstrate time entanglement, measurements in complementary time bases are required. This can be achieved by sending optical fields in unbalanced interferometers serving as time-bin analyzers, as suggested by Franson [35]. In our case, we use the IFC as a time-bin analyzer by preparing an AFC with a storage time of $\tau_{IFC} = 2$ μs in both spatial modes. The AFC structure acts on the single photons as a beam splitter with a delay line in one output, i.e., a part of an unbalanced Mach-Zehnder interferometer [4,36,37]. This provides a convenient and robust time-bin analyzer [36], without the need of phase stabilizing interferometers with several hundred meters path length difference. In the IFC, each Stokes and anti-Stokes photon can be either transmitted (early time bin E) or stored in the AFC and retrieved as an AFC echo after a time τ_{IFC} (late time bin L). The phase Φ_S (Φ_{AS}) between the early and late time bin can be tuned by changing the center frequency of the AFC with respect to the Stokes (anti-Stokes) photons [16]. A phase shift of 2π is achieved with a frequency detuning of Δ.

The coincidence histogram between Stokes and anti-Stokes photon detections after the time-bin analyzers, as a function of the $T_S + T_{AS}$ time will be thus composed of three peaks. One corresponds to the coincidences between transmitted Stokes and anti-Stokes [labeled $|E_S E_{AS}\rangle$ in panel (d) of Fig. 1] and it thus lays at $T_S + T_{AS} = \tau_{MC}$. One builds up with the coincidences between Stokes and anti-Stokes photons when both undergo AFC storage in the IFC, $|L_S L_{AS}\rangle$. Consequently, it will appear at $T_S + T_{AS} = \tau_{MC} + 2\tau_{IFC}$. The central peak featured in Fig. 1(d) at $T_S + T_{AS} = \tau_{MC} + \tau_{IFC}$ is the sum of two contributions: the coincidences between transmitted Stokes photons and stored anti-Stokes photons ($|E_S L_{AS}\rangle$) and those between stored Stokes photons and transmitted anti-Stokes photons ($|L_S E_{AS}\rangle$). If these two processes are indistinguishable and coherent (which requires, e.g., equal AFC echo efficiency in the IFC for both photons), they will be able to interfere. By selecting only the central peak, the correlation between Stokes and anti-Stokes photons can be
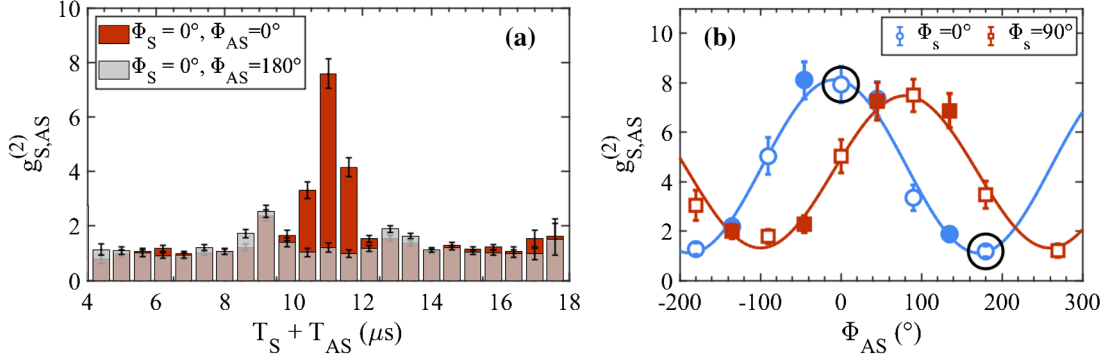
FIG. 3. (a) Examples of $g_{S,AS}^{(2)}$ between Stokes and anti-Stokes photons when an AFC with $\tau_{IFC} = 2~\mu s$ is prepared in both the Stokes and the anti-Stokes mode in the IFC. The cases of constructive (darker bars) and destructive (lighter bars) interference are shown. For both measurements, the integration time is 10 h, approximately. (b) Interference fringes measured by tuning the frequency of the anti-Stokes filter AFC (i.e., by tuning Φ_{AS}) in two different bases, selected by changing the frequency of the filter AFC for the Stokes photon. The circled points are the ones related to Fig. 3(a). The filled points are those used to calculate the S parameter (integration time 6.5 h per point). The remaining data point are the result of 5.5 h of integration each.

interpreted as coming from the postselected entangled state $(1/\sqrt{2})(|E_S L_{AS}\rangle + e^{i\theta}|L_S E_{AS}\rangle)$, where $\theta = \Phi_S - \Phi_{AS}$ [4]. This photonic state results from the postselected light-matter entangled state $(1/\sqrt{2})[a_S^\dagger(T)a_{SW}^\dagger(T) + a_S^\dagger(T')a_{SW}^\dagger(T')]|0_S 0_{SW}\rangle$ where T and T' are separated in time by τ_{IFC}, set by the analyzing interferometer. In our experiments, we tailor the finesse of the AFC structures in the IFC such that the amplitude of the transmitted and stored pulses are comparable (approximately 30% of the input pulses).

Figure 3(a) shows examples of $g_{S,AS}^{(2)}$ between Stokes and anti-Stokes photons when both pass through an AFC in the IFC. The constructive (dark bars) and destructive (light bars) interference cases are reported as obtained by fixing the Stokes phase shift $\Phi_S = 0°$, and the anti-Stokes phase shift Φ_{AS} to 0° and 180°, respectively. As expected, the two histograms differ in the area around $T_S + T_{AS} = 11~\mu s$. The value of $g_{S,AS}^{(2)}$ for constructive interference is 7.6 ± 0.5, lower than the value measured before the time-bin analyzers. This is due to the fact that there is an intrinsic loss in the

IFC ($\eta_{IFC} = 30\%$), and that the noise from different temporal modes is summed up.

In Fig. 3(b), we show the results of two photon interference measurements in different bases, obtained by tuning the anti-Stokes phase shift for two different values of Φ_S. The visibility is $(75.9 \pm 4.6)\%$ for $\Phi_S = 0°$ and $(70.1 \pm 4.4)\%$ for $\Phi_S = 90°$ showing evidence of entanglement. To further assess quantum entanglement, we perform an experiment probing the violation of the Clauser, Horne, Shimony, and Holt (CHSH) inequality [38]. We measure thus the coincidence histograms in 16 different settings to calculate the S parameter as a function of $T_S + T_{AS}$ as

$$S = E(\alpha, \beta) + E(\alpha', \beta) + E(\alpha, \beta') - E(\alpha', \beta'), \quad (3)$$

where α and α' (β and β') are two different phase choices for the Stokes (anti-Stokes) photons arm, and the dependency on $T_S + T_{AS}$ has been dropped for simplicity. The different terms of Eq. (3) are built from the coincidences C in a time bin $\Delta t = 600$ ns as follows:

$$E(\alpha, \beta) = \frac{C(\alpha, \beta) + C(\alpha + \pi, \beta + \pi) - C(\alpha, \beta + \pi) - C(\alpha + \pi, \beta)}{C(\alpha, \beta) + C(\alpha + \pi, \beta + \pi) + C(\alpha, \beta + \pi) + C(\alpha + \pi, \beta)}.$$

Figure 4 shows the resulting S parameters as a function of $T_S + T_{AS}$ when the phase values are fixed to $\alpha = 0°$, $\alpha' = 90°$, $\beta = 45°$, and $\beta' = 135°$. As expected, the maximum violation is obtained for $T_S + T_{AS} = \tau_{MC} + \tau_{IFC} = 11~\mu s$ where we measure $S = 2.15 + -0.07$, which surpasses the classical bound of 2 by more than 2 standard deviations. We also investigated the S parameter as a function of the coincidence window Δt, showing that higher violations can be obtained for smaller Δt, at the

expense of a lower coincidence count rate and read-out efficiency [31].

These measurements show that the Stokes and anti-Stokes photons are entangled in time. Consequently, as the conversion spin wave to anti-Stokes photon is a local operation, this also demonstrates entanglement between a photon and the spin-wave stored in the crystal.

We have shown that a solid-state device can emit pairs of entangled photons with an embedded quantum memory for
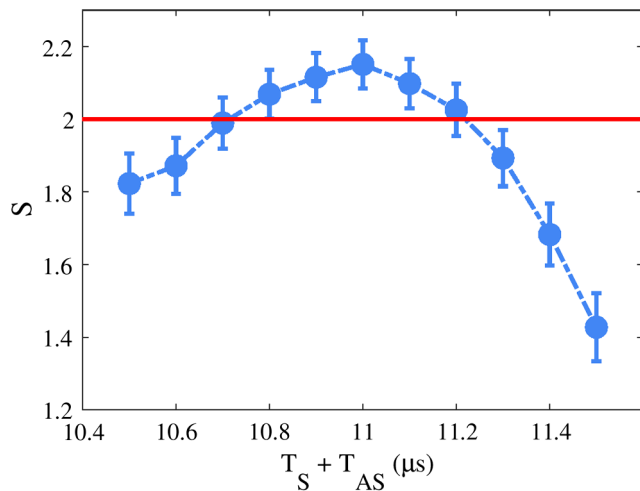
FIG. 4. Bell inequality S parameter measured as a function of $T_S + T_{\mathrm{AS}}$. The red line denotes the threshold $S = 2$ for violating the CHSH inequality.

one of the photons. Moreover, the quality of the entanglement is high enough to enable a violation of a Bell inequality, making our device suitable for applications in quantum communication. With improved performances [31], this device could be an important resource for the implementation of temporally multiplexed quantum repeaters. It could also serve as a platform for investigating high-dimensional entanglement in time between light and matter.

[1] H. J. Kimble, Nature (London) **453**, 1023 (2008).
[2] N. Sangouard, C. Simon, H. de Riedmatten, and N. Gisin, Rev. Mod. Phys. **83**, 33 (2011).
[3] C. Simon, H. de Riedmatten, M. Afzelius, N. Sangouard, H. Zbinden, and N. Gisin, Phys. Rev. Lett. **98**, 190503 (2007).
[4] C. Clausen, I. Usmani, F. Bussières, N. Sangouard, M. Afzelius, H. de Riedmatten, and N. Gisin, Nature (London) **469**, 508 (2011).
[5] E. Saglamyurek, N. Sinclair, J. Jin, J. A. Slater, D. Oblak, F. Bussières, M. George, R. Ricken, W. Sohler, and W. Tittel, Nature (London) **469**, 512 (2011).
[6] M. Afzelius, N. Gisin, and H. de Riedmatten, Phys. Today **68**, No. 12, 42 (2015).
[7] L.-M. Duan, M. D. Lukin, J. I. Cirac, and P. Zoller, Nature (London) **414**, 413 (2001).
[8] D. N. Matsukevich, T. Chanelière, M. Bhattacharya, S.-Y. Lan, S. D. Jenkins, T. A. B. Kennedy, and A. Kuzmich, Phys. Rev. Lett. **95**, 040405 (2005).
[9] H. de Riedmatten, J. Laurat, C. W. Chou, E. W. Schomburg, D. Felinto, and H. J. Kimble, Phys. Rev. Lett. **97**, 113603 (2006).
[10] S. Chen et al., Phys. Rev. Lett. **99**, 180505 (2007).
[11] Y.-F. Pu, N. Jiang, W. Chang, H.-X. Yang, C. Li, and L.-M. Duan, Nat. Commun. **8**, 15359 (2017).
[12] R. Chrapkiewicz, M. Dabrowski, and W. Wasilewski, Phys. Rev. Lett. **118**, 063603 (2017).
[13] R. Inoue, N. Kanai, T. Yonehara, Y. Miyamoto, M. Koashi, and M. Kozuma, Phys. Rev. A **74**, 053809 (2006).
[14] P. Farrera, G. Heinze, and H. de Riedmatten, Phys. Rev. Lett. **120**, 100501 (2018).
[15] R. Riedinger, S. Hong, R. A. Norte, J. A. Slater, J. Shang, A. G. Krause, V. Anant, M. Aspelmeyer, and S. Gröblacher, Nature (London) **530**, 313 (2016).
[16] M. Afzelius, C. Simon, H. de Riedmatten, and N. Gisin, Phys. Rev. A **79**, 052329 (2009).
[17] N. Sinclair et al., Phys. Rev. Lett. **113**, 053603 (2014).
[18] P. Sekatski, N. Sangouard, N. Gisin, H. de Riedmatten, and M. Afzelius, Phys. Rev. A **83**, 053840 (2011).
[19] P. M. Ledingham, W. R. Naylor, J. J. Longdell, S. E. Beavan, and M. J. Sellars, Phys. Rev. A **81**, 012301 (2010).
[20] P. M. Ledingham, W. R. Naylor, and J. J. Longdell, Phys. Rev. Lett. **109**, 093602 (2012).
[21] K. R. Ferguson, S. E. Beavan, J. J. Longdell, and M. J. Sellars, Phys. Rev. Lett. **117**, 020501 (2016).
[22] K. Kutluer, M. Mazzera, and H. de Riedmatten, Phys. Rev. Lett. **118**, 210502 (2017).
[23] C. Laplane, P. Jobez, J. Etesse, N. Gisin, and M. Afzelius, Phys. Rev. Lett. **118**, 210501 (2017).
[24] G. Heinze, C. Hubrich, and T. Halfmann, Phys. Rev. Lett. **111**, 033601 (2013).
[25] M. P. Hedges, J. J. Longdell, Y. Li, and M. J. Sellars, Nature (London) **465**, 1052 (2010).
[26] G. Corrielli, A. Seri, M. Mazzera, R. Osellame, and H. de Riedmatten, Phys. Rev. Applied **5**, 054013 (2016).
[27] A. Seri, G. Corrielli, D. Lago-Rivera, A. Lenhard, H. de Riedmatten, R. Osellame, and M. Mazzera, Optica **5**, 934 (2018).
[28] A. Seri, A. Lenhard, D. Rieländer, M. Gündoğan, P. M. Ledingham, M. Mazzera, and H. de Riedmatten, Phys. Rev. X **7**, 021028 (2017).
[29] M. Gündoğan, P. M. Ledingham, K. Kutluer, M. Mazzera, and H. de Riedmatten, Phys. Rev. Lett. **114**, 230501 (2015).
[30] A. Kuzmich, W. P. Bowen, A. D. Boozer, A. Boca, C. W. Chou, L.-M. Duan, and H. J. Kimble, Nature (London) **423**, 731 (2003).
[31] See Supplemental Material at http://link.aps.org/supplemental/10.1103/PhysRevLett.123.030501 for more details about the experimental setup, additional characterization of the entanglement generation and measurements, as well as a discussion about read-out efficiency, which includes Refs. [32–34].

[32] N. Maring, D. Lago-Rivera, A. Lenhard, G. Heinze, and H. de Riedmatten, Optica **5**, 507 (2018).

[33] M. Zhong, M. P. Hedges, R. L. Ahlefeldt, J. G. Bartholomew, S. E. Beavan, S. M. Wittig, J. J. Longdell, and M. J. Sellars, Nature (London) **517**, 177 (2015).

[34] M. Afzelius and C. Simon, Phys. Rev. A **82**, 022310 (2010).

[35] J. D. Franson, Phys. Rev. Lett. **62**, 2205 (1989).

[36] P. Jobez, Ph. D. thesis, University of Geneva, No. Sc. 4856, 2015.

[37] N. Maring, P. Farrera, K. Kutluer, M. Mazzera, G. Heinze, and H. de Riedmatten, Nature (London) **551**, 485 (2017).

[38] J. F. Clauser, M. A. Horne, A. Shimony, and R. A. Holt, Phys. Rev. Lett. **23**, 880 (1969).